

1 Observations of infrared radiative cooling in the thermosphere on 2 daily to multiyear timescales from the TIMED/SABER instrument

3
4 Martin G. Mlynczak, *NASA Langley Research Center, Hampton, VA*

5 Linda A. Hunt, *SSAI, Hampton, VA*

6 B. Thomas Marshall, *GATS Inc., Newport News, VA*

7 F. Javier Martin-Torres, *Jet Propulsion Laboratory, Pasadena, CA*

8 Christopher J. Mertens, *NASA Langley Research Center, Hampton, VA*

9 James M. Russell III, *Hampton University, Hampton, VA*

10 Ellis E. Remsberg, *NASA Langley Research Center, Hampton, VA*

11 Manuel López-Puertas, *IAA, Granada, Spain*

12 Richard Picard, *AFRL, Hanscom AFB, MA*

13 Jeremy Winick, *AFRL, Hanscom AFB, MA*

14 , *ARCON Corp., Waltham, MA*

15 R. Earl Thompson, *GATS Inc., Newport News, VA*

16 Larry L. Gordley, *GATS Inc., Newport News, VA*

17
18 **Abstract.** We present observations of the infrared radiative cooling by carbon dioxide (CO₂) and
19 nitric oxide (NO) in Earth's thermosphere. These data have been taken over a period of 7 years
20 by the SABER instrument on the NASA TIMED satellite and are the dominant radiative cooling
21 mechanisms for the thermosphere. From the SABER observations we derive vertical profiles of
22 radiative cooling rates (W m⁻³), radiative fluxes (W m⁻²), and radiated power (W). In the period
23 from January 2002 through January 2009 we observe a large decrease in the cooling rates,
24 fluxes, and power consistent with the declining phase of solar cycle 23. The power radiated by
25 NO during 2008 when the Sun exhibited few sunspots was nearly one order of magnitude
26 smaller than the peak power observed shortly after the mission began. Substantial short-term
27 variability in the infrared emissions is also observed throughout the entire mission duration.
28 Radiative cooling rates and radiative fluxes from NO exhibit fundamentally different latitude
29 dependence than do those from CO₂, with the NO fluxes and cooling rates being largest at high
30 latitudes and polar regions. The cooling rates are shown to be derived relatively independent of
31 the collisional and radiative processes that drive the departure from local thermodynamic
32 equilibrium (LTE) in the CO₂ 15 μm and the NO 5.3 μm vibration-rotation bands. The observed
33 NO and CO₂ cooling rates have been compiled into a separate dataset and represent a climate
34 data record that is available for use in assessments of radiative cooling in upper atmosphere
35 general circulation models.

36 37 **1. Introduction**

38 The terrestrial thermosphere and mesosphere have been the least explored regions of
39 Earth's atmosphere. They are too high for in-situ measurements from aircraft or balloons. Rocket
40 or ground-based measurements on a global basis are not practical and do not provide the suite of
41 measurements required for a complete characterization of these regions. In the middle 1990s
42 remote sensing technology became sufficiently advanced to enable comprehensive satellite

1 observations of these regions of the atmosphere. The NASA Thermosphere-Ionosphere-
2 Mesosphere Energetics and Dynamics (TIMED) mission was developed to explore the Earth's
3 atmosphere above 60 km altitude and was launched in December 2001. A fundamental goal of
4 the mission is to quantify the energy budget of mesosphere and thermosphere. One of four
5 instruments on the TIMED mission, the Sounding of the Atmosphere using Broadband Emission
6 Radiometry (SABER) instrument, was specifically designed to measure the energy budget of the
7 mesosphere and lower thermosphere [Mlynczak, 1996; 1997].

8 The SABER instrument is a 10-channel limb scanning radiometer. It scans the Earth's
9 limb continuously recording profiles of infrared radiance ($\text{W m}^{-2} \text{sr}^{-1}$) from the atmosphere in
10 discrete spectral intervals [Russell *et al.*, 1999]. The specific wavelength bands observed by
11 SABER were chosen so that a variety of data products could be retrieved or derived, including
12 kinetic temperature, ozone, water vapor, carbon dioxide, atomic oxygen, atomic hydrogen, rates
13 of energy deposition, rates of energy loss, and rates of radiative heating and cooling. To this end,
14 SABER measures two of the three key infrared emissions that govern radiative cooling of the
15 atmosphere above 100 km: nitric oxide (NO) at $5.3 \mu\text{m}$ [Kockarts, 1980] and carbon dioxide
16 (CO_2) at $15 \mu\text{m}$ [Curtis and Goody, 1956]. The third emission, the fine structure line of atomic
17 oxygen (O^3P) at $63 \mu\text{m}$ [Bates, 1951] is not measured by SABER but has been observed by the
18 CRISTA instrument that flew twice in the 1990s on the Space Shuttle [Grossman *et al.*, 2000]
19 and by numerous rocket experiments [Grossman and Vollmann, 1997] and even by high altitude
20 balloons [Mlynczak *et al.*, 2004]. The SABER dataset is the first global, long-term, and
21 continuous record of the NO and CO_2 emissions from the thermosphere.

22 The SABER dataset is now seven years in length and has already provided some basic
23 insight into the heat budget of the thermosphere on a variety of timescales. Mlynczak *et al.*,

1 [2003; 2005; 2007a] have reported the observed nature of the nitric oxide emission in the
2 thermosphere in response to geomagnetic storm events, demonstrating a “thermostat” effect in
3 which the infrared emission rapidly and efficiently removes storm energy deposited into the
4 thermosphere and thus returns it to its original state in a short period of time. The long-term
5 effects of the declining phase of solar cycle 23 were clearly evident in the NO emission in less
6 than 5 years [Mlynczak *et al.*, 2007b] and 9-day periodicities in both the NO and CO₂ emissions
7 have been related to the occurrence of coronal holes on the Sun [Mlynczak *et al.*, 2008].

8 The purpose of this paper is to further examine variability in the NO 5.3 μm and CO₂ 15
9 μm emissions with the SABER dataset. In particular, the extent of solar minimum conditions
10 during the end of solar cycle 23 offers a unique opportunity to study the radiative cooling in the
11 thermosphere under exceptionally quiescent conditions. We also examine the infrared emissions
12 as a function of latitude and altitude. In addition, the newest version of the SABER data set
13 (v1.07) is used in this study. Lastly, the results presented here form a climate data record for the
14 thermosphere useful for assessing general circulation models of the upper atmosphere. The
15 cooling rate data may be obtained from the authors upon request.

16 In the next section we review the data processing methodology. In Section 3 we present
17 the results in the order of the processing: vertical profiles of radiative cooling (W m⁻³), fluxes of
18 infrared emission (W m⁻²), and radiated power (W). Discussions on the fundamentally different
19 roles of cooling by NO and CO₂ are given. In Section 4 we discuss the sensitivity of the results to
20 parameters in the SABER retrieval algorithms and in Section 5 we give a summary.

21 **2. Derivation of Infrared Parameters**

22 The fundamental SABER measurement is the infrared radiance (W m⁻² sr⁻¹) measured in
23 the limb viewing geometry as a function of tangent altitude. The instrument scans the

1 atmosphere from approximately 400 km tangent altitude down to 5 km below the hard Earth
2 surface, recording an infrared radiance sample every 0.4 km. The NO 5.3 μm emission is
3 observed as high as 300 km during periods of intense geomagnetic storms. The CO₂ 15 μm
4 emission is typically observed up to 139 km. Approximately 1400 profiles of infrared emission
5 are obtained for each of the 10 SABER channels in one day. During the limb scan between 100
6 and 200 km (the nominal range reported in this paper) the TIMED spacecraft moves
7 approximately 1 degree of latitude. The nominal instantaneous field of view of the instrument is
8 2 km at the tangent point on the Earth's limb.

9 The TIMED satellite is in an orbit inclined 74 degrees with respect to the equator. The
10 SABER instrument views perpendicular to the spacecraft velocity vector. In order to keep the
11 SABER instrument within its allowable range of operating temperatures, the TIMED spacecraft
12 executes a rotation about its yaw axis every 60 days to keep the Sun from illuminating the
13 instrument's thermal radiator. While in the "northward" viewing mode the SABER instrument
14 views from approximately 83°N to 55°S. After the yaw maneuver the instrument views from
15 approximately 55°N to 83°S. This operational scenario results in the regions between 55°N and
16 55°S being viewed continuously while the regions above 55 degrees latitude are viewed
17 continuously for 2 months every other yaw cycle, i.e., two months of viewing followed by a 2
18 month gap, followed by 2 months of viewing, etc. This process repeats exactly the same
19 temporal gaps in both hemispheres every year.

20 In the results below for zonal mean cooling rates and fluxes we present annual averages.
21 Because of the SABER viewing geometry, the averages are over 12 months only between +/- 55
22 degrees in latitude (corresponding to 82% of atmospheric area). In the regions poleward of 55
23 deg we average the six months of available data every year. While not truly annual, these 6-

1 month averages cover locally two months during winter, two months during fall, one month
2 during spring, and one month during summer. There is no obvious discontinuity in the cooling
3 rates and fluxes shown in the figures below and we believe the results are substantially
4 representative of the annual behavior, although comparisons with models are required to verify
5 this assertion. More than 50,000 individual cooling rate profiles are observed in a 6-month period
6 poleward of 55 degrees.

7 The derivation of the infrared radiative cooling rates (W m^{-3}) is accomplished by
8 different techniques for the NO and CO₂ emissions owing to the different opacities of these
9 molecules in the limb view, and to account for the different physical processes that result in
10 emission and cooling of the atmosphere by these molecules. To further study the energy balance
11 we vertically integrate each profile of radiative cooling to obtain the flux (W m^{-2}) of energy
12 exiting the thermosphere. The fluxes are then zonally integrated to provide an estimate of the
13 equator-to-pole distribution of radiative cooling which is central to the large-scale atmospheric
14 circulation. The fluxes are then integrated with respect to area around a latitude circle, and then,
15 from pole-to-pole, to estimate the total power (W) radiated each day by the thermosphere. These
16 analysis procedures with SABER data are given in *Mlynczak et al.*, [2005, 2007a]. We will
17 review these here since there are fundamental differences in the approaches for analyzing the
18 (more) optically thick 15- μm band of CO₂ and the optically thin 5.3 μm band of NO.

19 **2.1 NO(v) at 5.3 μm**

20 Infrared emission from NO is a substantial cooling mechanism throughout the
21 thermosphere. Due to the low atmospheric density, the vibration-rotation bands of the NO
22 molecule depart from local thermodynamic equilibrium (LTE) [e.g., *Funke and López -Puertas,*
23 2000]. The NO vibrational states are excited primarily by collisions with atomic oxygen with a

1 rate coefficient of $4.2 \times 10^{-11} \exp(-2700/T) \text{ cm}^3 \text{ s}^{-1}$ [Hwang *et al.*, 2003], where T is the kinetic
2 temperature. By comparison, excitation by the absorption of terrestrial radiation is several orders
3 of magnitude smaller. Nitric oxide is also formed through a series of chemical reactions that
4 excite high-lying vibration-rotation bands especially during geomagnetic storms. These have
5 been observed near 195 km by the CIRRIS-1A instrument that flew on the Space Shuttle [Dothe
6 *et al.*, 2002; Sharma *et al.*, 1996].

7 The approach to deriving the NO cooling rates from SABER observations has been
8 discussed by Mlynczak *et al.* [2005], and is reviewed here. The emission from nitric oxide is in
9 the weak line limit of radiative transfer. The equation of radiative transfer describing a transition
10 in the weak line limit is given in the limb view by the expression:

$$11 \quad R(H_o) = \frac{hc\nu}{4\pi} \sum_x V(x) dx \quad (1)$$

12 where $R(H_o)$ is the measured spectrally integrated radiance ($\text{W m}^{-2} \text{ sr}^{-1}$) at tangent altitude H_o , h
13 is Planck's constant, c the speed of light, ν the frequency of the transition (wavenumbers, cm^{-1}),
14 $V(x)$ is the volume emission rate of photons at the tangent altitude, and dx is a path element
15 along the limb line of sight. An Abel or geometric inversion may be applied to the measured
16 radiance profile, assuming spherical symmetry about the tangent point, yielding a vertical profile
17 of the rate of emission of energy per unit volume (W m^{-3}). For optically thin transitions such as
18 those of NO, the energy escapes the thermosphere completely: half of the energy is emitted to
19 space, half to the atmosphere below.

20 As the SABER instrument is a filter radiometer, the initial result from the Abel inversion
21 process is a cooling/emission rate that is weighted by the filter bandpass of the instrument. To
22 obtain the total rate of emission, a correction factor is applied to the measured in-band emission
23 rate to obtain the emission rate for the entire band. The correction factor varies substantially with

1 altitude for NO and has been computed from extensive model calculations discussed in *Mlynczak*
2 *et al.* [2005]. The correction factor was verified through observations of NO spectra made by the
3 MIPAS instrument [*Gardner et al.*, 2006] on the EnviSat satellite. Surprisingly, *Mlynczak et al.*
4 [2005] found relatively small variation in this correction (“unfilter”) factor from quiescent to
5 geomagnetically disturbed conditions.

6 In the results presented below we treat the entire emission from NO as cooling the
7 atmosphere. Terrestrial (“earthshine”) emission is insignificant as an excitation mechanism of
8 nitric oxide vibrations, relative to collisions with atomic oxygen. The results from *Dothe et al.*
9 [2002] indicate that emission from high-lying NO vibrational levels is still well below that of the
10 fundamental ($\nu = 1$ to $\nu = 0$) band. The correction factor applied to the SABER measured in-
11 band emission rate accounts for out-of-band contributions of the 2-1 and 3-2 vibrational states as
12 well. Potential refinements to this process will be discussed in Section 5.

13 **2.2 CO₂(ν_2) at 15 μm**

14 In this section we outline the method to compute the cooling rates for the CO₂ 15 μm ν_2
15 fundamental band transition, with upper state designation CO₂(01¹0). Later in the paper we will
16 examine the role of cooling by the first hot band in this mode, i.e., the CO₂ (02²0 \rightarrow 01¹0)
17 transition. Above 100 km, the CO₂ 15 μm fundamental band is not exactly optically thin, but
18 neither is it very optically thick. Because of this, derivation of the cooling rates for the CO₂
19 molecule is not as straightforward as for NO. Specifically, the absence of true weak line radiative
20 transfer precludes application of an Abel or geometric inversion to simply derive a
21 cooling/emission rate profile. In addition, radiative exchange with other layers of the atmosphere
22 occurs, although absorption of radiation from the lower atmosphere is relatively small [*López-*
23 *Puertas and Taylor*, 2001]. Only emission resulting from collisional excitation results in a

1 cooling of the atmosphere. In addition, due to the opacity, not all emission escapes to space or
2 the atmosphere below, unlike NO. We must therefore employ a technique to compute the true
3 cooling of the atmosphere given these constraints.

4 The SABER experiment measures emission in the ν_2 bending mode of CO₂ at 15 μm for
5 the purpose of retrieving the kinetic temperature of the atmosphere. The 15 μm bands are also
6 responsible for the radiative cooling of the atmosphere. As with NO, the vibration-rotation bands
7 of carbon dioxide depart from local thermodynamic equilibrium (LTE) in the upper mesosphere
8 and thermosphere. The SABER temperature derivation includes detailed modeling of the
9 collisional and radiative processes that drive the observed transitions from LTE [*Mertens et al.*,
10 2001]. Specifically, the Curtis matrix approach [*López-Puertas et al.*, 1986a, b] is employed in
11 the SABER non-LTE modeling and temperature derivation process and directly yields the
12 infrared radiative cooling rates in Kelvin per day. These cooling rates computed at each iteration
13 step are output and stored as standard data products upon convergence of the temperature
14 retrieval.

15 To derive the local rate $\partial Q/\partial t$ of radiative cooling in W m^{-3} for CO₂ at a given altitude we
16 apply the first law of thermodynamics:

$$17 \quad \frac{\partial Q}{\partial t} = \rho C_p \frac{\partial T}{\partial t} \quad (2)$$

18 C_p is the heat capacity at constant pressure, ρ the density, and $\partial T/\partial t$ the derived radiative cooling
19 rate in Kelvin per day. From the ideal gas law this can be written as:

$$20 \quad \frac{\partial Q}{\partial t} = \frac{p C_p}{T R} \frac{\partial T}{\partial t} \quad (3)$$

21 In Equation 3, R is the gas constant. This approach to computing cooling rates and fluxes was
22 successfully applied in the stratosphere by *Mlynczak et al.*, [1998.] In our present analyses the

1 pressure, temperature, and $\partial T/\partial t$ are obtained from the SABER v1.07 dataset. Although the
2 effect is small, we also include the variation of the ratio C_p/R with altitude to be consistent with
3 that used in the SABER data processing, thus accounting for the effects of atomic oxygen on C_p .

4 **3. Results**

5 **3.1 Cooling rates for NO at 5.3 μm**

6 We begin by examining the cooling rates (W m^{-3}) for NO over the seven years of data to
7 date. The SABER instrument began routine operations in mid-January 2001. To maintain
8 SABER's orientation on the "cold" side of the spacecraft, the TIMED spacecraft undergoes a
9 180-degree yaw maneuver every 60 days, as dictated by the progression through local time in the
10 satellite's 74 degree inclined orbit. Thus in a year the spacecraft executes a series of six yaw
11 maneuvers, allowing the same progression of local time to be repeated each year. In all figures
12 presented below, unless noted otherwise, we display annual averages for each of the seven "yaw
13 years" that have been observed to date. Each "yaw year" runs from mid-January to the next mid-
14 January. So the year 2002 runs from January 2002 to January 2003, and so on.

15 Shown in Figure 1 are the zonally averaged, annual mean cooling rates in W m^{-3} for NO
16 observed by SABER from January 2002 through January 2009, i.e., yaw years 2002 through
17 2008. There are two features immediately obvious from the data. First, the maximum cooling
18 rates occur at high latitudes near the poles, implying a strong geomagnetic influence. Second, the
19 magnitude of the cooling rates visibly decreases each year in the series from 2002 through 2008.
20 This decrease is concurrent with the declining phase of solar cycle 23. At the altitude of the
21 cooling rate peak poleward of 60 degrees, the cooling rates decrease by a factor of ~ 4.5 . The
22 cooling rate is observed to decrease throughout the entire range from 100 to 200 km over the 7
23 years of observations. By 2008 there is very little emission observed by SABER above 180 km.

1 For carbon dioxide we find a different picture of cooling rates in the plots shown in
2 Figure 2. Whereas the NO cooling rates showed a clear equator-to-pole enhancement throughout
3 the thermosphere, CO₂ exhibits a relatively small gradient in equator to pole cooling above 105
4 km. Below 105 km there is evidence of strong cooling near the poles and also at the equator. The
5 equatorial enhancement in CO₂ cooling is visible in all 7 years of data. Similar to the NO
6 cooling, a decrease in the strength of the CO₂ cooling over the 7 years is also visible in Figure 2.

7 Figures 1 and 2 demonstrate a decrease in radiative cooling by NO and CO₂ in the
8 thermosphere over the last seven years. This decrease is consistent with a decrease in the
9 temperature of the thermosphere which affects both NO and CO₂, although the temperature
10 sensitivity of the NO emission is substantially larger than for CO₂. The strength of radiative
11 cooling is proportional to $\exp(\Delta E/k_B T)$ where ΔE is the photon energy, k_B is Boltzmann's
12 constant, and T is the kinetic temperature. Since ΔE for NO is about 2.8 times larger than for
13 CO₂, NO emission has a substantially larger sensitivity to a specific change in temperature.
14 Decreases in atomic oxygen over the solar cycle also contribute to the decline in infrared cooling
15 from both molecules.

16 The NO cooling will also be affected directly by a decrease in the NO density that would
17 be expected to occur during the declining phase of the solar cycle, while the CO₂ concentration
18 has only a small anticipated source due to continued anthropogenic buildup and virtually no
19 known sinks that are due to the solar cycle. Thus the larger observed changes in NO cooling as
20 compared with CO₂ are due to a combination of a larger sensitivity of the emission to
21 temperature and to an overall decrease in the NO abundance. The influence of solar cycle on
22 radiative cooling is best shown in Figures 3a and 3b which depict the annual, global average
23 cooling in 2002 through 2008, for NO and CO₂, respectively. For NO in Figure 3a we have

1 extended the plot up to 250 km altitude, illustrating the extent of nitric oxide emission during
2 solar maximum (and also the sensitivity of the SABER instrument.) The NO cooling shows a
3 continued and marked decrease for each year in the sequence. The largest decrease is in the
4 global average cooling by nitric oxide, approximately a factor of ~6.5 at the peak. In contrast, the
5 CO₂ cooling has decreased by about 35% over the solar cycle. The smaller sensitivity of the CO₂
6 cooling to the solar cycle is due to the fact that the CO₂ emissions originate in the lower (more
7 dense) atmosphere, to the smaller sensitivity of the CO₂ emission to temperature changes, and to
8 a lack of sinks of CO₂ abundance.

9 **3.2 Fluxes of Exiting Longwave Radiation**

10 The next step in the process of assessing the radiative cooling is to integrate vertically the
11 cooling rate profiles and obtain the flux of longwave radiation that exits the thermosphere. We
12 choose to call this the ‘exiting’ longwave radiation (ELR) in analogy to the ‘outgoing’ longwave
13 radiation (OLR) used in studies of the Earth’s tropospheric climate. The difference is that the
14 OLR all leaves the planet whereas only about half of the ELR leaves the planet while the rest is
15 absorbed in the atmosphere below the thermosphere. The range of vertical integration is 100 to
16 200 km for NO and 100 to 139 km for CO₂.

17 Shown in Figures 4 and 5 are polar stereographic plots of ELR for NO in the northern
18 and southern hemispheres, respectively. The scale on the color bar runs from 0.0 to 1.0
19 milliwatts per square meter. These ELR plots show the annual average fluxes of radiation exiting
20 the thermosphere between 2002 and 2008 and correspond to the same time periods as the cooling
21 rates shown in Figure 1. Clearly visible are larger fluxes near the poles in all years, with fluxes in
22 2002 and 2003 peaking in excess of 0.8 milliwatts per square meter. Also evident is a dramatic
23 decrease in flux from 2002 to 2008. In 2002 in most of each hemisphere the ELR exceeds 0.3

1 milliwatts per square meter. In 2008 the ELR over most of the globe is well below 0.07
2 milliwatts per square meter. Thus the effect of the declining phase of solar cycle 23 is clearly
3 evident in the ELR.

4 Figures 6 and 7 show the ELR for the northern and southern hemispheres from 2002 to
5 2008 for CO₂. The scale runs from 0.8 to 2.4 milliwatts per square meter. The CO₂ fluxes are
6 substantially larger than those for NO and are reflective of the role CO₂ plays in cooling the
7 lower (and more dense) thermosphere. Evident in these figures is a general decrease from 2002
8 to 2008. However, as evidenced by the emission rates of energy in Figures 2 and 3b, the decrease
9 in the ELR for CO₂ is much less than that for NO, on a percentage basis. As with the NO
10 emission, the CO₂ ELR is always largest in polar regions, reflecting the high latitude
11 enhancements in CO₂ cooling shown in Figure 2 in the lower thermosphere. The tropical
12 enhancement in cooling by CO₂ shown in Figure 2 is also evident in the fluxes in Figures 6 and
13 7. The tropical enhancement in fact exhibits 4 alternating maxima and minima in each year,
14 perhaps implying a dynamical (tidal?) effect. The tropical maximum decreases substantially from
15 solar maximum in 2002 to solar minimum in 2008. The extent of large fluxes of ELR from CO₂
16 also decreases at the pole, but there is still substantial cooling, although over a reduced area, in
17 2008.

18 **3.2.1 Zonal Mean Fluxes of Exiting Longwave Radiation**

19 Next we zonally average the ELR for NO and CO₂ shown in Figures 4 through 7 to
20 display the annual average ELR as a function of latitude. In Figures 8 and 9 we show the annual
21 average ELR for each year 2002 through 2008 for NO and CO₂, respectively. The ELR is plotted
22 versus the sine of latitude so that the abscissa is proportional to atmospheric area. The first
23 feature that stands out from examination of both figures is that starting in 2003, the ELR

1 decreases each year compared with the previous year. The decrease is generally uniform with
2 latitude although the ELR in the high latitude northern hemisphere in 2003 is comparable to that
3 in 2002, and again comparable in 2004 and 2005. The ELR for NO decreases by about a factor of
4 8 in the low to mid-latitudes, while the ELR for CO₂ decreases by about 30% over the same
5 range of latitudes. The general decrease in ELR from 2002 to 2008 is again an indication of the
6 effects of the declining phase of solar cycle 23. However, the fact that the ELR decrease is not
7 identical at all latitudes indicates that the effects of solar variability are not necessarily uniform
8 throughout the thermosphere.

9 A second feature that stands out upon examination of Figures 8 and 9, and which is
10 hinted at in Figures 1 and 2, is that the equator-to-pole gradient of the ELR is different for NO
11 and CO₂, with the gradient for NO being larger than for CO₂. The equator-to-pole gradient of net
12 heating (solar heating minus radiative cooling) of the atmosphere is a major factor that drives the
13 large-scale circulation of the thermosphere, and the atmosphere in general. The fact that the
14 gradient is larger in NO and becomes lesser over the solar cycle as both temperature and the NO
15 abundance decrease implies a potential link between chemistry, dynamics, and radiation
16 governed by the abundance of NO.

17 Shown in Figure 10 is the zonally averaged ELR for the sum of NO and CO₂. As shown
18 for the individual ELR terms, the combined ELR is larger in all years at high latitudes than at
19 low latitudes in both hemispheres. Because the ELR is the vertically integrated radiative cooling
20 rate, the results illustrated in Figure 9 demonstrate that the high latitude and polar thermosphere
21 is cooled more strongly by infrared radiation than at low and tropical latitudes. This result is
22 fundamental. Larger radiative cooling at high latitudes than at low latitudes is known to exist in
23 the mesosphere [*Mlynczak, 2000*] and the stratosphere [*Mlynczak et al., 1998*]. However, in the

1 troposphere, the opposite is true, i.e., the outgoing longwave radiation is larger at the equator
2 than at the poles [*VonderHaar and Suomi, 1969*]. The results of this and previous studies show
3 that the upper atmosphere cools in a fundamentally different manner than the troposphere.

4 Another property of the ELR evident from Figures 10 is that in addition to the general
5 decrease in ELR over the 7 years of data, the equator-to-pole gradient of radiative cooling has
6 weakened substantially over this time period. While the decrease in ELR implies that the
7 thermosphere has cooled, and in the case of NO, that the abundance of NO has also likely
8 decreased, the weakening of the equator-to-pole gradient of cooling implies that the large-scale
9 dynamics may have also weakened considerably during this time. These infrared emissions thus
10 provide solid evidence as to changes in the thermal structure, photochemistry, and dynamics of
11 the thermosphere, and hint strongly at a coupling between NO chemistry and the large-scale
12 dynamics and transport in the thermosphere.

13 **3.3 Global Radiative Power**

14 The last parameter that we will calculate is the global radiative power (Watts) emitted by
15 CO₂ and NO. These have been previously been shown by *Mlynczak et al. [2007b, 2008]* in
16 examining long and short term variations in the energy balance of the thermosphere. We obtain
17 the total global power by zonally integrating the fluxes of ELR shown above, and then
18 integrating the power in each latitude bin from pole-to-pole. To compute the power poleward of
19 55 degrees in the hemisphere not being observed, we follow *Mlynczak et al. [2005]* in assuming
20 the ratio of the power between the equator and 55 degrees latitude and between 55 degrees
21 latitude and the pole is the same in both hemispheres. This process provides a measure of the
22 total global power radiated by NO and CO₂ on a daily basis. The power for the full 7 years of
23 data is shown in Figure 11. What is evident is the overall decline of radiated power consistent

1 with the declining phase of solar cycle 23. In addition there is substantial short-term variability in
2 both the NO and CO₂ emissions, that has previously been linked to geomagnetic phenomena
3 [Mlynczak *et al.*, 2008]. Large increases in radiative power associated with extreme geomagnetic
4 events (e.g., the October 2003 Halloween superstorm event) are evident. In addition, in 2008, the
5 values of NO power reach very low values, nearly a factor of 10 lower (when averaged over a
6 60-day yaw cycle) than at the beginning of the mission. During 2008 the Sun exhibited no
7 sunspots for over 200 days. We suggest that the SABER data over this time period offer an
8 excellent resource for studying the influence of the Sun on the climate of the upper atmosphere.

9 The CO₂ cooling rates, fluxes of ELR, and radiative power shown above are all computed
10 for the fundamental band of the CO₂ molecule. In the SABER temperature retrieval process more
11 than 20 vibration-rotation bands (including isotopic bands) are considered and the non-LTE
12 problem is solved for each band, including cooling rates in Kelvin per day. To verify that the
13 fundamental band dominates the CO₂ cooling we also computed cooling rates (W m⁻³), fluxes of
14 ELR, and radiated power (W) for the first hot band of the CO₂ bending mode. Shown in Figure
15 12 is a time series of the power radiated by the CO₂ fundamental and first hot bands. It is clear
16 from this figure that the fundamental band dominates the CO₂ 15 μm thermospheric cooling and
17 that the first hot band is about 3.5% of the fundamental band emission. However, the decrease in
18 NO emission over the solar cycle is such that, between 100 and 200 km, the radiated power from
19 the first hot band of CO₂ rivals that of NO in 2008, on an annual average basis, although the
20 emissions do peak in substantially different regions of the atmosphere. Table 1 lists the annual
21 average power for CO₂ (fundamental and first hot bands) and NO for the 2002 through 2008
22 “yaw years.”

23 **4.0 Sensitivity to non-LTE parameters in the SABER algorithms**

1 A key question in the analysis and derivation of the CO₂ cooling rates in W m⁻³ is the
2 extent to which the results are sensitive to the non-LTE processes and the modeling of these
3 processes in the SABER temperature, pressure, and cooling rate (K/day) derivation in the
4 operational SABER data processing algorithms. We demonstrate that the derived cooling rates,
5 in W m⁻³, as a function of altitude, are essentially insensitive to the non-LTE parameters in the
6 SABER algorithms, because the rate of emission is essentially constrained by the SABER
7 radiance measurements. Furthermore, the ELR fluxes and radiated power are similarly
8 insensitive since they are derived directly from the cooling rate in W m⁻³.

9 The primary process by which CO₂ cools the atmosphere, analogous to NO, is by
10 radiative emission subsequent to collisional excitation by an oxygen atom. In 1970 P. Crutzen
11 postulated that this process would be important in cooling the thermosphere, and since that time,
12 substantial efforts have been expended both in the laboratory [e.g. *Castle et al.*, 2006] and in
13 analyzing atmospheric observations [e.g., *Rodgers et al.*, 1992; *López-Puertas et al.*, 1992] to
14 determine the rate coefficient for the process



16 Literature values for this rate “O/CO₂” coefficient range over a factor of 4 from approximately 6
17 x 10⁻¹² cm³s⁻¹ [*Sharma and Wintersteiner*, 1990] to ~ 1.4 x 10⁻¹² cm³s⁻¹ [*Khvorostovskaya et al.*,
18 2002]. The SABER temperature algorithms incorporate the Sharma and Wintersteiner value for
19 this rate coefficient.

20 In the SABER algorithms, the modeling of the non-LTE processes depends on the
21 provision of the O/CO₂ rate coefficient, the atomic oxygen density, and the CO₂ abundance.
22 Atomic oxygen is provided from the NRL-MSIS model [*Picone et al.*, 2002] and the CO₂
23 abundance is provided from the Whole Atmosphere Community Climate Model (WACCM)

1 model [R. Garcia, National Center for Atmospheric Research, private communication, 2006].
2 With these provisions, temperature is retrieved and constrained by the measured radiance at 15
3 μm by the SABER instrument [*Mertens et al.*, 2001].

4 To assess the effect the O/CO₂ rate coefficient on the derived cooling rates in W m^{-3} from
5 CO₂, we ran 7 complete days of the v1.07 operational SABER algorithm in which we reduced
6 the rate coefficient by a factor of 4 uniformly at all altitudes. This is also equivalent, in the non-
7 LTE modeling, to varying the atomic oxygen concentration by a factor of 4, or the product of
8 atomic oxygen and the rate coefficient by a factor of 4. We computed the cooling rates (W m^{-3}),
9 ELR fluxes (W m^{-2}) and power (W) for each of the test days and compared with the original
10 values. The results showed that the cooling rates (W m^{-3}), fluxes, and power did not show much
11 variation despite a huge variation in the key non-LTE rate coefficient. There are large changes in
12 temperature, pressure, density, and cooling rates in Kelvin per day, but not in the cooling rate in
13 W m^{-3} . An example is shown in Figure 13.

14 The explanation for the relative insensitivity of the cooling rate (W m^{-3}) is that decreasing
15 the O/CO₂ rate coefficient results in a decrease in the population of excited CO₂ molecules in the
16 algorithm. However, the SABER algorithm must compensate to match the measured radiance. It
17 does this primarily by increasing the temperature and pressure. An increase in temperature
18 increases the population of vibrationally excited CO₂ molecules by the Boltzmann factor as a
19 consequence of detailed balance. The algorithm thus works to provide the correct number of
20 excited CO₂ molecules to create the emission rate necessary to match the measured radiance.
21 Thus, the cooling from CO₂ in W m^{-3} is essentially unchanged. Our approach is found to be quite
22 robust and in fact provides the cooling rates (in W m^{-3}) essentially independent of the non-LTE
23 model parameters used to produce the SABER data products. The previously mentioned fact that

1 radiative excitation from the lower atmosphere is not very large also contributes to this result.
2 We note the NO cooling rates in W m^{-3} are also derived independent of any modeled non-LTE
3 processes by virtue of the weak line inversion and because the NO emission is essentially
4 generated solely by collisions with atomic oxygen.

5 The relative insensitivity to non-LTE processes of the derived cooling rates in W m^{-3}
6 presented here is a substantial result. The accuracy of the derived cooling rates is then tied
7 directly to the absolute calibration of the SABER instrument through the measured radiances.
8 The cooling rates also represent a data set that can be used to test directly cooling rate
9 parameterizations in upper atmosphere general circulation models [e.g., *Qian et al.*, 2009]. The
10 model parameterizations are very sensitive to the non-LTE processes including the rate
11 coefficient for energy transfer between atomic oxygen and carbon dioxide because they have no
12 constraint (e.g., a measured radiance). Through such comparisons the long-standing
13 discrepancies between renderings of the key non-LTE parameters may be resolved. The relative
14 insensitivity to the large change in the rate coefficient also suggests that the dataset of cooling
15 rates can form a climate data record [*National Research Council*, 2004] for the thermosphere.

16 **5. Discussion and Summary**

17 We have presented 7 years of observations of the radiative cooling in the thermosphere as
18 observed by the SABER instrument on the TIMED mission. The cooling rates in W m^{-3} are
19 derived for emission from CO_2 at $15 \mu\text{m}$ and NO at $5.3 \mu\text{m}$. The emissions exhibit both short and
20 long-term variations that illustrate the sensitivity of the thermosphere on time scales ranging
21 from daily to the 11 year solar cycle. The cooling by NO is substantially more variable than that
22 of CO_2 due to a greater sensitivity to temperature and to a much larger variability of NO density

1 with solar activity. Decreases in atomic oxygen between 2002 and 2008 likely contribute to the
2 observed decrease in both NO and CO₂ cooling.

3 The variability of the cooling has several fundamental consequences. First, the larger
4 equator-to-pole gradient in cooling by NO, and its variability, implies a potential link to
5 dynamics and transport as the equator-to-pole gradient in net heating drives the large-scale
6 circulation. The observed weakening of the equator-to-pole gradient in radiative cooling over
7 these seven years is a strong indication that the large-scale thermospheric dynamics have also
8 weakened. In addition, the larger cooling at the poles than at low latitudes in the thermosphere is
9 consistent with the observed cooling in the mesosphere and stratosphere, but is opposite of what
10 is observed in the troposphere. Thus the entire upper atmosphere behaves in a fundamentally
11 different manner than the troposphere with regards to radiative cooling as a function of latitude.

12 We have also shown that the cooling rates derived herein are essentially insensitive to the
13 parameters and rate coefficients used to compute the non-LTE populations of the carbon dioxide
14 molecule. This is because the retrieval algorithm must match the measured radiance, and thus
15 will produce enough excited CO₂ molecules to accomplish this, whether by increasing
16 temperature or pressure (or both) to accomplish the result. Further study on the sensitivity to the
17 carbon dioxide abundance used in the retrieval is warranted. We would expect perhaps only
18 minor sensitivity to CO₂ abundance given the relative insensitivity to a factor of 4 change in the
19 primary process responsible for cooling, and that we do not expect the CO₂ used in the SABER
20 retrieval to be off by a factor of 4. At this time we estimate the cooling rates for CO₂ emission to
21 be accurate to better than 15%.

22 In the case of NO, the assumption is that the observed emission is essentially all cooling,
23 and that the Abel inversion and correction factors applied to determine the total band emission

1 are sufficient. There are uncertainties in the derived cooling, most notably in the process used to
2 derive the full band cooling from the measured in-band emission. This correction (“unfilter”)
3 factor is essentially a function of the rotational temperature of the NO vibration-rotation bands.
4 For the v1.07 SABER data we do not make a correction for the rotational temperature as a
5 function of time. As the thermosphere cools, we would expect the rotational temperature to
6 decrease and thus there is a possibility that the correction factor to generate the total cooling rates
7 would also change. If that were the case, the correction factor would in general decrease,
8 implying that the changes with solar cycle may be larger than presented above. These
9 possibilities will be investigated in future studies by the SABER science team. We also estimate
10 the cooling rates due to NO to be accurate to better than 15%. This estimate is based on the
11 accuracy of the SABER radiometric calibration (1%), the possible effects of rotational
12 temperature uncertainties (~ 10%), and on emissions that may not be properly accounted for in
13 correcting for the spectral response filter function of the SABER NO channel (~ 10%).
14 Assuming these uncertainties are uncorrelated, the root-sum-square of these is conservatively ~
15 15%.

16 In closing we suggest that the dataset of radiative cooling of the thermosphere by NO and
17 CO₂ constitutes a first climate data record for the thermosphere. The length of the data record
18 and the apparent lack of dependence of the data products on model parameters results in an
19 accurate set of parameters that can be used to conduct fundamental tests of general circulation
20 models of the thermosphere. The cooling rates, radiative fluxes, and radiated power can all be
21 compared against model calculations. This should enable tests of model chemistry and physics
22 and in principle, resolve long-standing issues with regards to the parameterization of radiative
23 cooling in these models. As the TIMED mission continues, these data derived from SABER will

1 become important in assessing long term changes due to the increase of carbon dioxide in the
2 atmosphere.

3 **Acknowledgement:** MGM would like to acknowledge continued support from the Science
4 Directorate at NASA Langley, from the NASA Heliophysics Division TIMED Project, and from
5 the NASA Heliophysics Division Guest Investigator Program.

6

1 **References**

2 Bates, D. R., The temperature of the upper atmosphere, *Proc. Phys. Soc.*, B64, 805-821, 1951.

3

4 Castle, K. J., K. M. Kleissas, J. M. Rhinehart, E. S. Hwang, and J. A. Dodd, Vibrational

5 relaxation of CO₂(v₂) by atomic oxygen, *J. Geophys. Res.*, 111, doi:10.1029/2006JA001736,

6 2006

7

8 Dothe, H., J. W. Duff, R. D. Sharma, and N. B. Wheeler, (2002), A model of odd nitrogen in the

9 aurorally dosed nighttime terrestrial thermosphere, *J. Geophys. Res.*, 107, (A6), 1071, doi:

10 10.1029/2001JA000143

11

12 Curtis, A. R., and R. M. Goody, Thermal radiation in the upper atmosphere, *Proc. Roy. Soc.*

13 *London Ser. A*, 236, 193, 1956.

14

15 Grossman, K. U., M. Kaufmann, and E. Gerstner, A global measurement of lower thermosphere

16 atomic oxygen densities, *Geophys. Res. Lett.*, 27, 1387-1390, 2000.

17

18 Grossman, K. U., and K. Vollmann, Thermal infrared measurements in the middle and upper

19 atmosphere, *Adv. Space Res.*, 19, 631-638, 1997.

20

21 Gardner J. L., B. Funke, M. G. Mlynczak, M. López-Puertas, F. J. Martín-Torres, J. M. Russell

22 III, S. M. Miller, R. D. Sharma, J. R. Winick (2007), Comparison of nighttime nitric oxide

1 5.3 μm emissions in the thermosphere measured by MIPAS and SABER, *J. Geophys. Res.*,
2 112, A10301, doi:10.1029/2006JA011984.
3
4 Funke, B., and M. López-Puertas (2000), Nonlocal thermodynamic equilibrium vibrational,
5 rotational, and spin state distribution of NO($v = 0, 1, 2$) under quiescent atmospheric
6 conditions, *J. Geophys. Res.*, 105(D4), 4409-4426
7
8 Hwang E. S., K. J. Castle, and J. A. Dodd, Vibrational relaxation of NO($v = 1$) by oxygen atoms
9 between 295 and 825 K, *J. Geophys. Res.*, 108 (A3), 1109, doi:10.1029/2002JA009688,
10 2003.
11
12 Khvorostovskaya, L. E., I. Y. Potekhin, G. M. Shved, V. P. Ogibalov, and T. V. Uzyukova
13 (2002), Measurement of the rate constant for quenching CO₂ [0110] by atomic oxygen at low
14 temperatures: Reassessment of the rate of cooling by the CO₂ 15- μm emission in the lower
15 thermosphere, *Atmos. Ocean. Phys.*, 38, 613– 624.
16
17 Kockarts, G., Nitric oxide cooling in the terrestrial thermosphere, *Geophys. Res. Lett.*, 7, 137-
18 140, 1980.
19
20 López-Puertas, M. and F. Taylor, Non-LTE Radiative Transfer in the Atmosphere, Series on
21 Atmospheric, Ocean and Planetary Physics, Vol. 3, World Scientific Publishing Company,
22 2002.
23

1 López-Puertas, M., M. A. López-Valverde, C. P. Rinsland, and M. R. Gunson (1992), Analysis of
2 the upper atmospheric CO₂ (ν₂) vibrational temperatures retrieved from ATMOS-Spacelab 3
3 observations, *J. Geophys. Res.*, 97, 20,469–20,478
4

5 López-Puertas, M., R. Rodrigo, A. Molina, and F. W. Taylor, A non-LTE radiative transfer
6 model for infrared bands in the middle atmosphere, I, Theoretical basis and application to the
7 CO₂ 15 μm bands, *J. Atmos. Terr. Phys.*, 48, 729-748, 1986a.
8

9 López -Puertas, M., R. Rodrigo, J. J. López-Moreno, and F. W. Taylor, A non-LTE radiative
10 transfer model for infrared bands in the middle atmosphere, II, CO₂ (2.7 and 4.3 μm) and
11 water vapour (6.3 μm) and N₂(1) and O, *J. Atmos. Terr. Phys.*, 48, 749-764, 1986b.
12

13 Mertens C. J., M. G. Mlynczak, M. López-Puertas, and E. E. Remsberg, Impact of non-LTE
14 processes on middle atmospheric water vapor retrievals from simulated measurements of 6.8
15 μ m Earth limb emission, *Geophys. Res. Lett.*, 29 (9), doi:10.1029/2001GL014590, 2002.
16

17 Mlynczak, M. G., F. Javier Martin-Torres, Christopher J. Mertens, B. Thomas Marshall, R. Earl
18 Thompson, Janet U. Kozyra, Ellis E. Remsberg, Larry L. Gordley, James M. Russell III, and
19 Thomas Woods, (2008), Solar-terrestrial coupling evidenced by periodic behavior in
20 geomagnetic indexes and the infrared energy budget of the thermosphere, *Geophys. Res.*
21 *Lett.*, 35, L05808, doi:10.1029/2007GL032620.
22

1 Mlynczak M. G., F. J. Martin-Torres, J. M. Russell III (2007a), Correction to “Energy transport
2 in the thermosphere during the solar storms of April 2002”, *J. Geophys. Res.*, 112, A02303,
3 doi:10.1029/2006JA012008.

4

5 Mlynczak, M. G., F. J. Martin-Torres, B. T. Marshall, E. Thompson, J. Williams, T. Turpin, D.
6 P. P. Kratz, J. M. Russell III, T. N. Woods, and L. L. Gordley (2007b), Evidence for a solar
7 cycle influence on the infrared energy budget and radiative cooling of the thermosphere, *J.*
8 *Geophys. Res.*, doi:10.1029/2006JA012194.

9

10 Mlynczak, M. G. et al., Energy transport in the thermosphere during the solar storm events of
11 April 2002, *J. Geophys. Res.*, 110, A12S25, doi:10.1029/2005JA011141, 2005.

12

13 Mlynczak M., et al., The natural thermostat of nitric oxide emission at 5.3 μ m in the
14 thermosphere observed during the solar storms of April 2002, *Geophys. Res. Lett.*, 30 (21),
15 2100, doi:10.1029/2003GL017693, 2003.

16

17 Mlynczak, M. G., A contemporary assessment of the middle atmosphere energy budget, in
18 Atmospheric Science Across the Stratopause, edited by D. Siskind, S. Eckermann, and M.
19 Summers, *Geophysical Monographs Series 123*, American Geophysical Union, p. 37-52,
20 2000.

21

1 Mlynczak, M. G., Mertens, C. J., R. R. Garcia, and R. W. Portmann, A detailed evaluation of the
2 stratospheric heat budget. II. Global radiation balance and diabatic circulations, *J. Geophys.*
3 *Res.*, 104, 6039-6066, 1999.

4

5 Mlynczak, M. G., Energetics of the mesosphere and lower thermosphere and the SABER
6 experiment, *Advances in Space Research*, Volume 20, Issue 6, 1997, Pages 1177-1183

7

8 Mlynczak, M. G., Energetics of the middle atmosphere: Theory and observation requirements,
9 *Advances in Space Research*, Volume 17, Issue 11, 1996, Pages 117-126

10

11 National Research Council, Climate data records from environmental satellites, National
12 Academy Press, ISBN 0-309-09168-3, National Academy Press, Washington, DC, 2004.

13

14 Picone J. M., A. E. Hedin, D. P. Drob, and A. C. Aikin, NRLMSISE-00 empirical model of the
15 atmosphere: Statistical comparisons and scientific issues, *J. Geophys. Res.*, 107 (A12), 1468,
16 doi:10.1029/2002JA009430, 2002.

17

18 Qian, L., S. Solomon, and M. G. Mlynczak, Model Simulation of Thermospheric Response to
19 Recurrent Geomagnetic Forcing, *J. Geophys. Res.*, submitted, 2009.

20

21 Overview of the SABER experiment and preliminary calibration results, James M. Russell III,
22 Martin G. Mlynczak, Larry L. Gordley, Joseph J. Tansock, Jr., and Roy W. Esplin, Proc.
23 SPIE 3756, 277 (1999).

1
2
3
4
5
6
7
8
9
10
11
12
13
14
15
16
17

Rodgers, C., F. Taylor, A. Muggeridge, M. López-Puertas, and M. López-Valverde (1992),
Local thermodynamic equilibrium of carbon dioxide in the upper atmosphere, *Geophys. Res. Lett.*, 19(6), 589-592.

Sharma, R. D., H. Dothe, F. von Esse, V. A. Kharchenko, Y. Sun, and A. Dalgarno, Production
of vibrationally and rotationally excited NO in the night time terrestrial thermosphere, *J. Geophys. Res.*, 101 (A9), 19,707-19,713, 1996.

Sharma, R., and P. Wintersteiner (1990), Role of carbon dioxide in cooling planetary
thermospheres, *Geophys. Res. Lett.*, 17(12), 2201-2204.

Vonder Haar, T. H., and V. E. Suomi, Measurements of the Earth's radiation budget from
satellites during a five-year period. Part I. Extended time and space means, *J. Atmos. Sci.*, 28,
305-314, 1969.

1
2
3
4
5
6
7

Table 1. Annual mean, global power (W) radiated from the thermosphere (100 to 200 km) by the carbon dioxide fundamental band, the carbon dioxide first hot band, and by nitric oxide, from 2002 through 2008.

Year	CO₂ Fundamental Power (10¹¹ W)	CO₂ First Hot Band Power (10¹¹ W)	NO ($\Delta v = 1$) Power (10¹¹ W)
2002	9.19	0.334	2.26
2003	8.85	0.332	1.94
2004	8.05	0.306	1.21
2005	7.69	0.306	0.947
2006	7.46	0.288	0.583
2007	6.97	0.267	0.407
2008	6.90	0.220	0.337

8
9

1 **Figure Captions**

2

3 **Figure 1.** Zonal average, annual mean cooling rates (W m^{-3}) for nitric oxide from 2002 through
4 2008.

5

6 **Figure 2.** Zonal average, annual mean cooling rates (W m^{-3}) for carbon dioxide from 2002
7 through 2008.

8

9 **Figure 3a.** Global annual average cooling rate profiles, solar maximum (2002) and solar
10 minimum (2008) and all years in between, for NO, derived from the cooling rates in Figure 1.

11

12 **Figure 3b.** Global annual average cooling rate profiles, solar maximum (2002) and solar
13 minimum (2008), for CO₂ derived from the cooling rates in Figure 2.

14

15 **Figure 4.** Annual average exiting longwave radiative flux (mW m^{-2}) for nitric oxide, northern
16 hemisphere, 2002 through 2008.

17

18 **Figure 5.** Annual average exiting longwave radiative flux (mW m^{-2}) for nitric oxide, southern
19 hemisphere, from 2002 to 2008.

20

21 **Figure 6.** Annual average exiting longwave radiative flux (mW m^{-2}) for carbon dioxide, northern
22 hemisphere, from 2002 to 2008.

23

1 **Figure 7.** Annual average exiting longwave radiative flux (mW m^{-2}) for carbon dioxide, southern
2 hemisphere, 2002 to 2008.

3

4 **Figure 8.** Annual mean, zonal average exiting longwave radiative flux (W m^{-2}) for nitric oxide,
5 2002 through 2008.

6

7 **Figure 9.** Annual average, zonal mean exiting longwave radiative flux (W m^{-2}) from carbon
8 dioxide at $15 \mu\text{m}$, 2002 through 2008.

9

10 **Figure 10.** Annual average, zonal mean exiting longwave radiative flux, (W m^{-2}), for nitric oxide
11 and carbon dioxide, 2002 through 2008.

12

13 **Figure 11.** Daily global power (W) emitted from the thermosphere by CO_2 (red) and NO (green)
14 between 100 km and 200 km altitude.

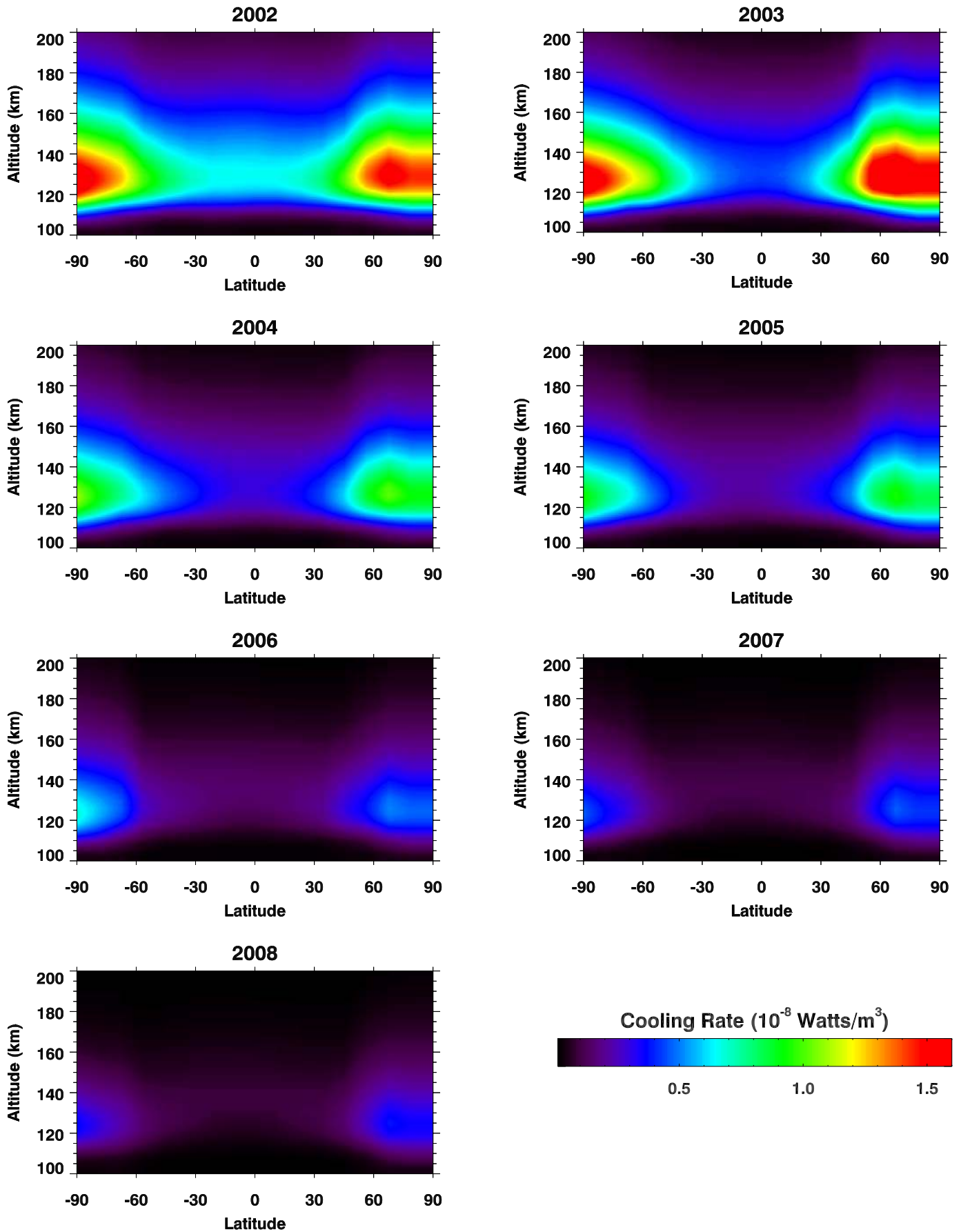
15

16 **Figure 12.** Daily global power (W) computed for CO_2 fundamental and first hot bands in the
17 thermosphere between 100 km and 140 km.

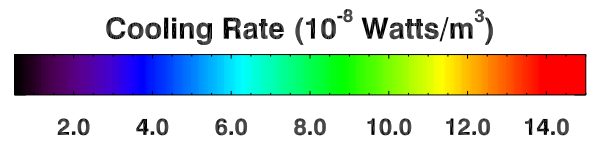
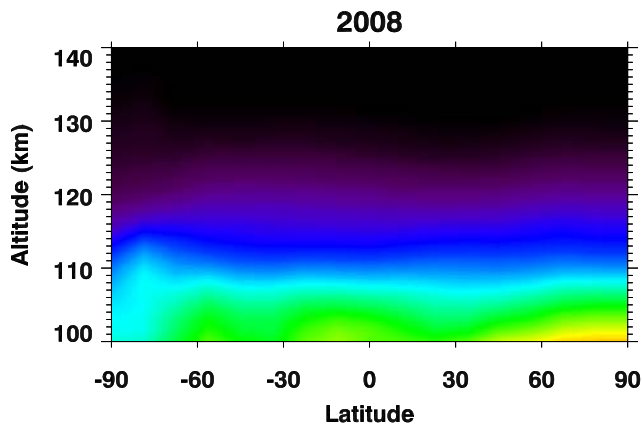
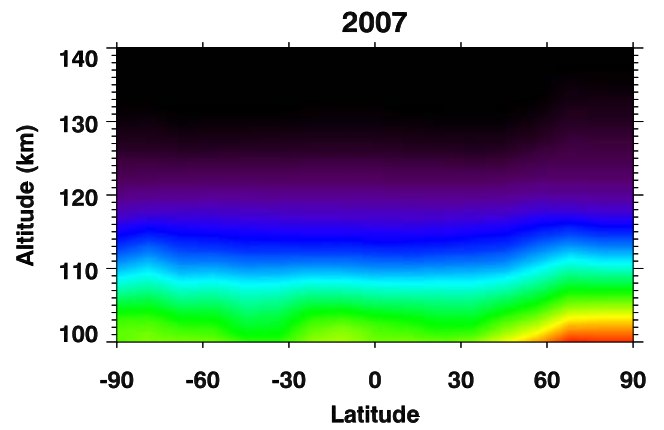
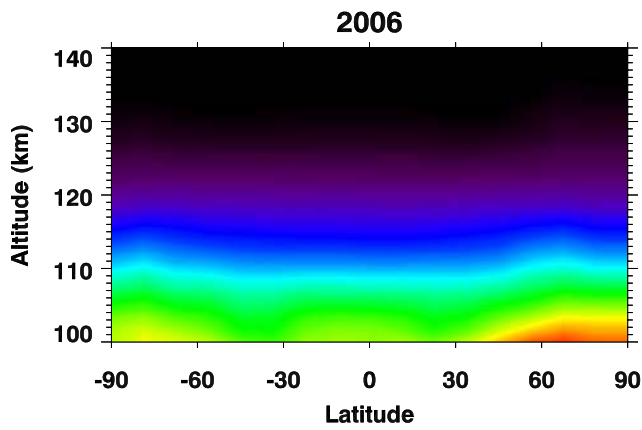
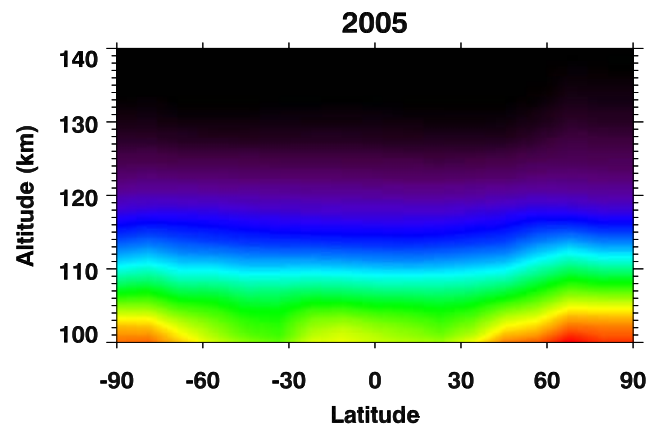
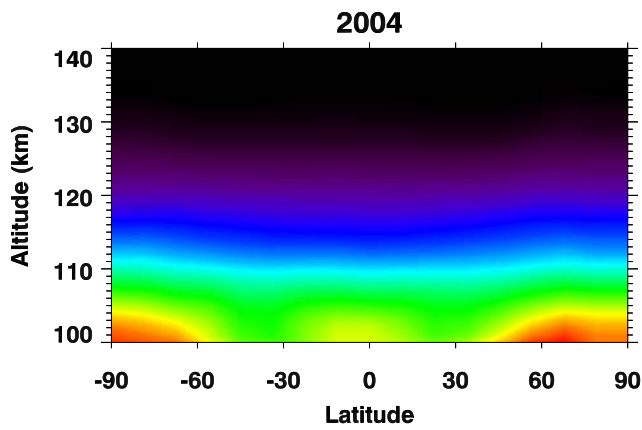
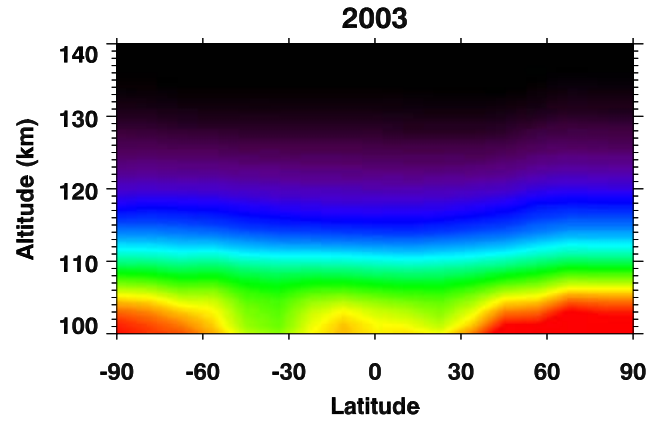
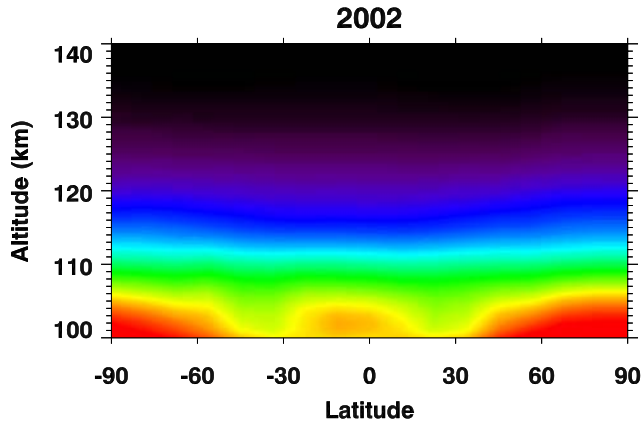
18

19 **Figure 13.** Results of SABER retrieved data products (radiative cooling rate in K/day; radiative
20 cooling rate in W m^{-3} ; kinetic temperature; pressure; and density), from the nominal retrieval
21 algorithm (green) and from a sensitivity test in which the quenching rate of vibrationally excited
22 carbon dioxide by atomic oxygen was reduced uniformly by a factor of 4 (red). The results show
23 that the cooling rate in W m^{-3} is essentially unchanged. See text for further explanation.

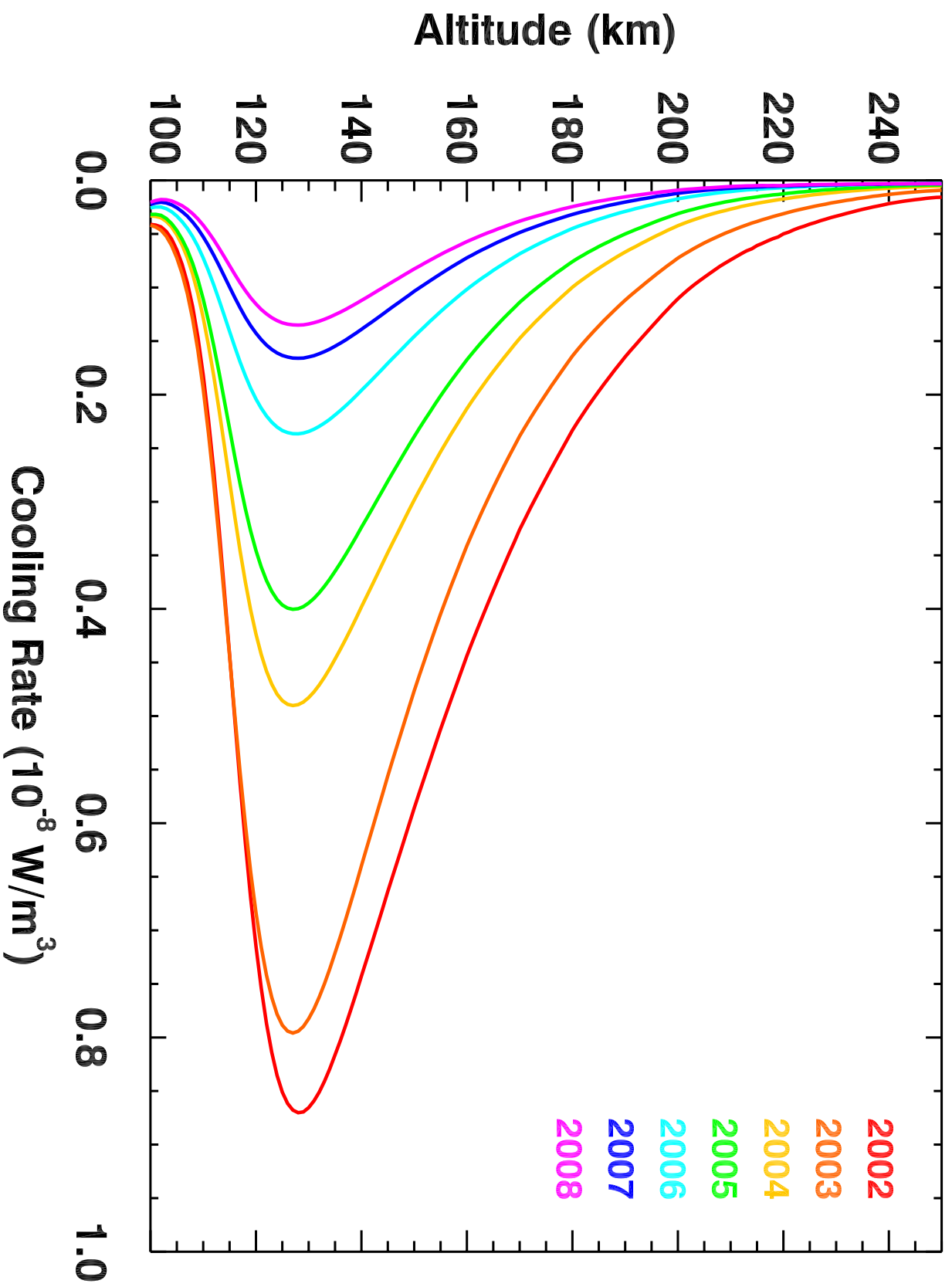
Nitric Oxide Annual Average Cooling Rate



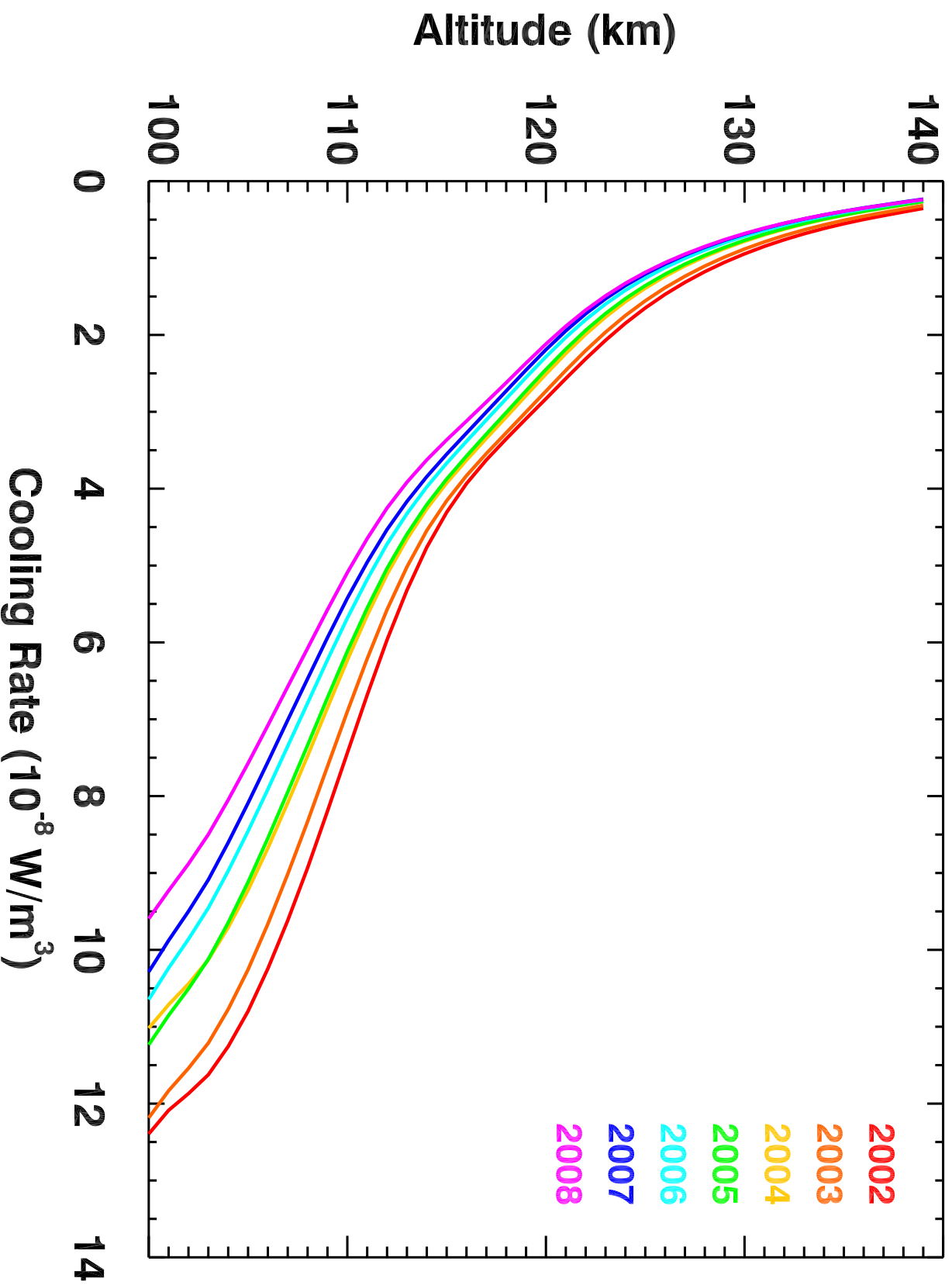
Carbon Dioxide Annual Average Cooling Rate



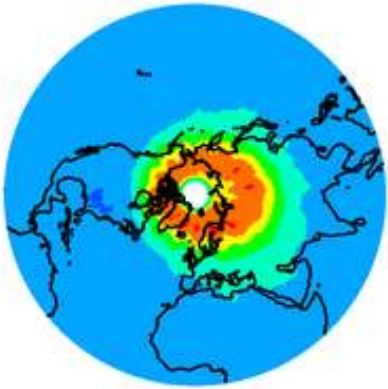
SABER NO Global Annual Average Cooling Rate



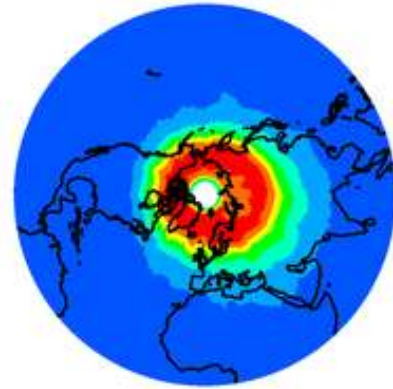
SABER CO2 Global Annual Average Cooling Rate



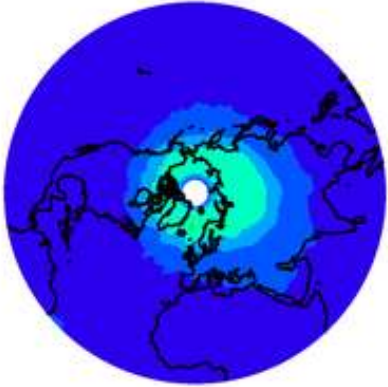
2002



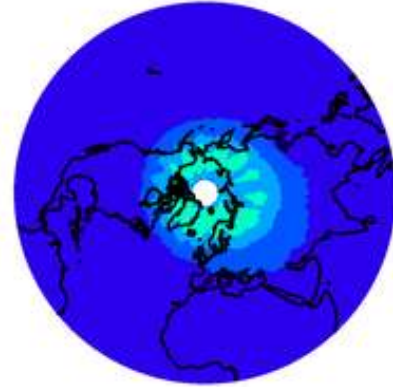
2003



2004



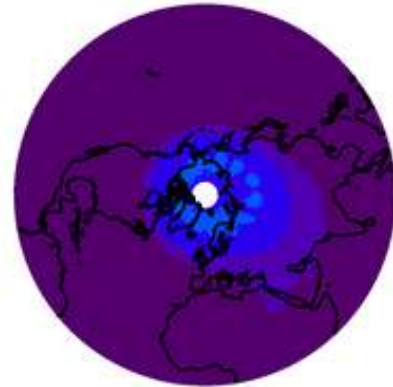
2005



2006



2007



2008



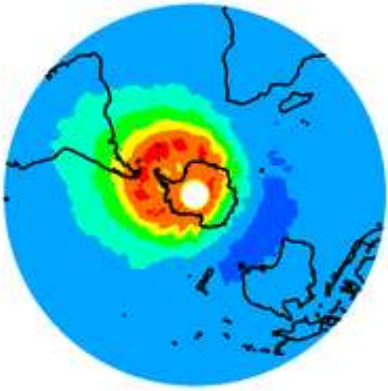
**ANNUAL AVERAGE NO INFRARED FLUX
Northern Hemisphere**

Milliwatts/m²

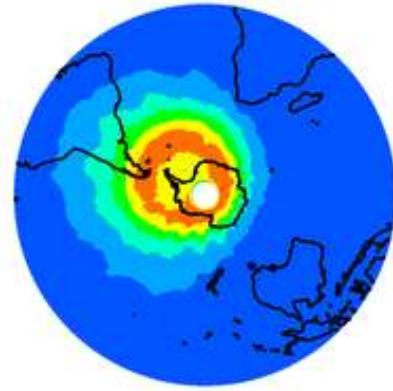


0.00 0.04 0.07 0.10 0.20 0.30 0.40 0.50 0.60 0.70 0.80 1.00

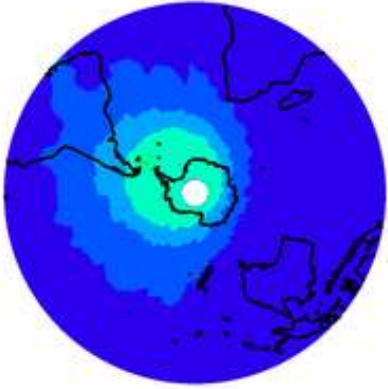
2002



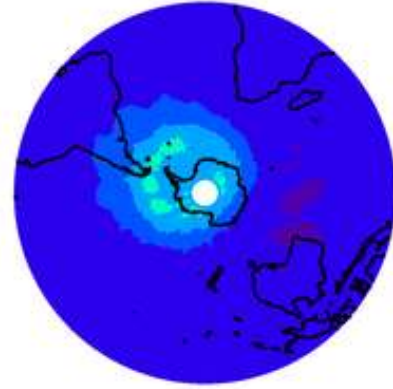
2003



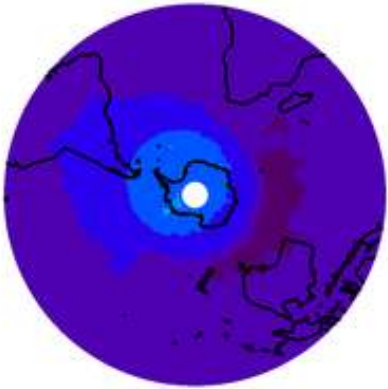
2004



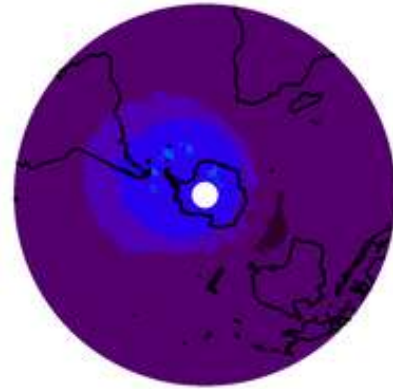
2005



2006



2007



2008



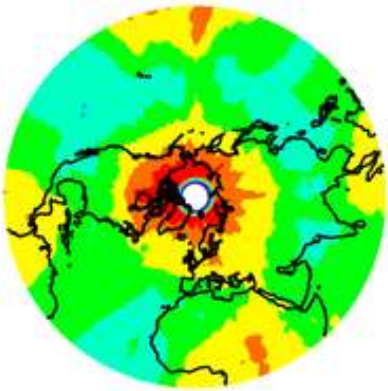
**ANNUAL AVERAGE NO INFRARED FLUX
Southern Hemisphere**

Milliwatts/m²

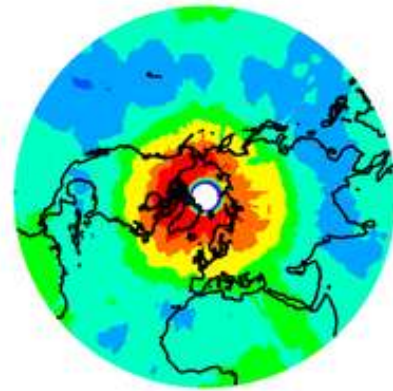


0.00 0.04 0.07 0.10 0.20 0.30 0.40 0.50 0.60 0.70 0.80 1.00

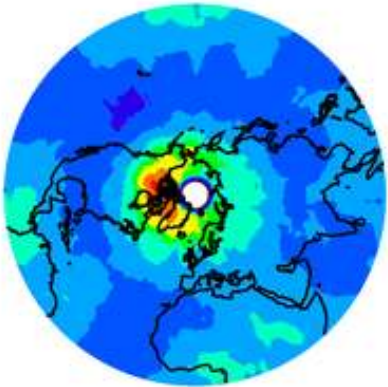
2002



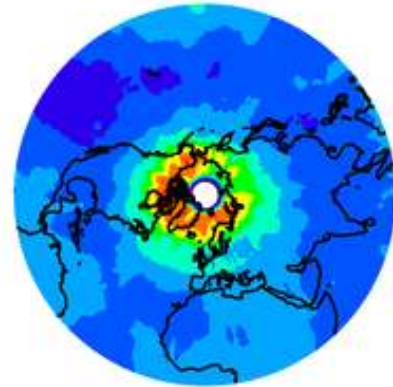
2003



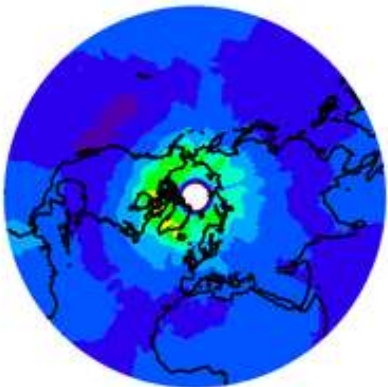
2004



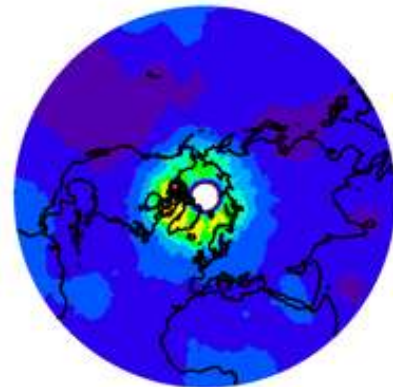
2005



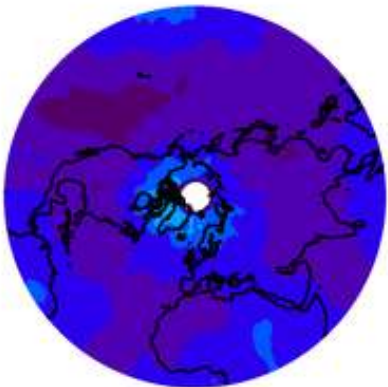
2006



2007



2008



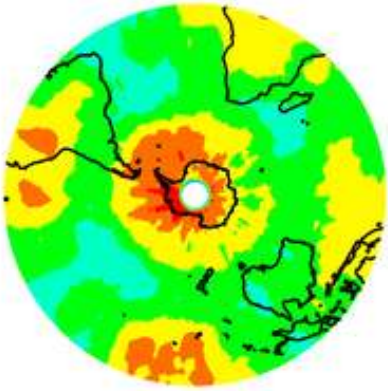
**ANNUAL AVERAGE CO2 INFRARED FLUX
Northern Hemisphere**

Milliwatts/m²

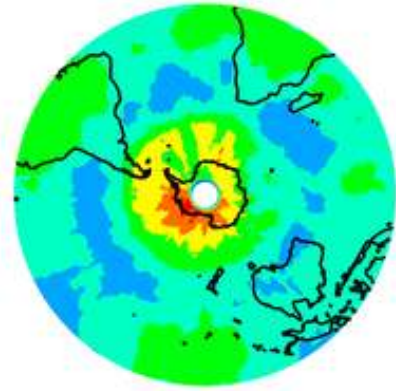


0.8 1.0 1.1 1.2 1.3 1.4 1.5 1.6 1.7 1.8 1.9 2.0 2.4

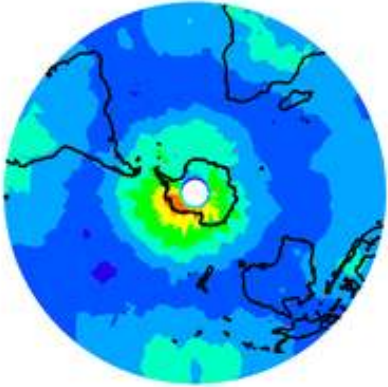
2002



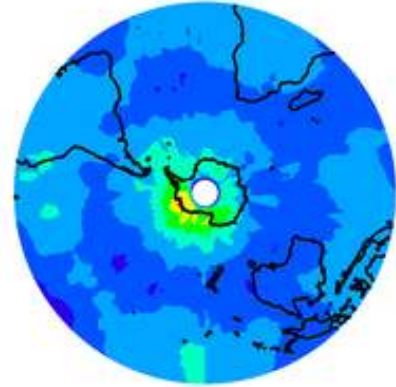
2003



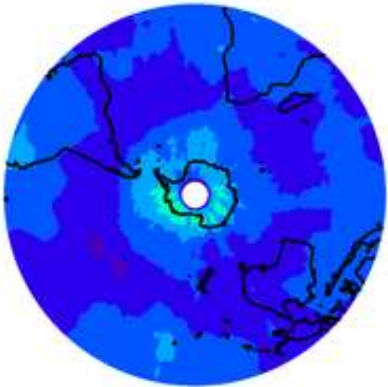
2004



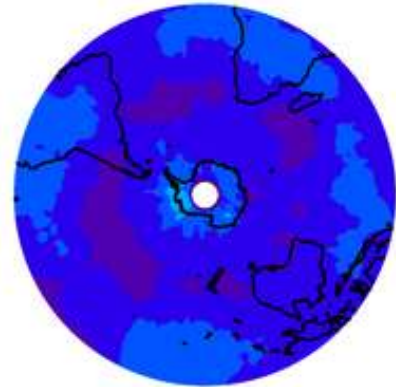
2005



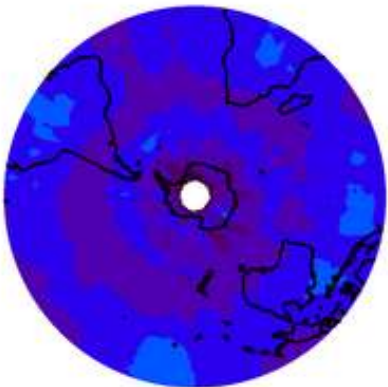
2006



2007



2008



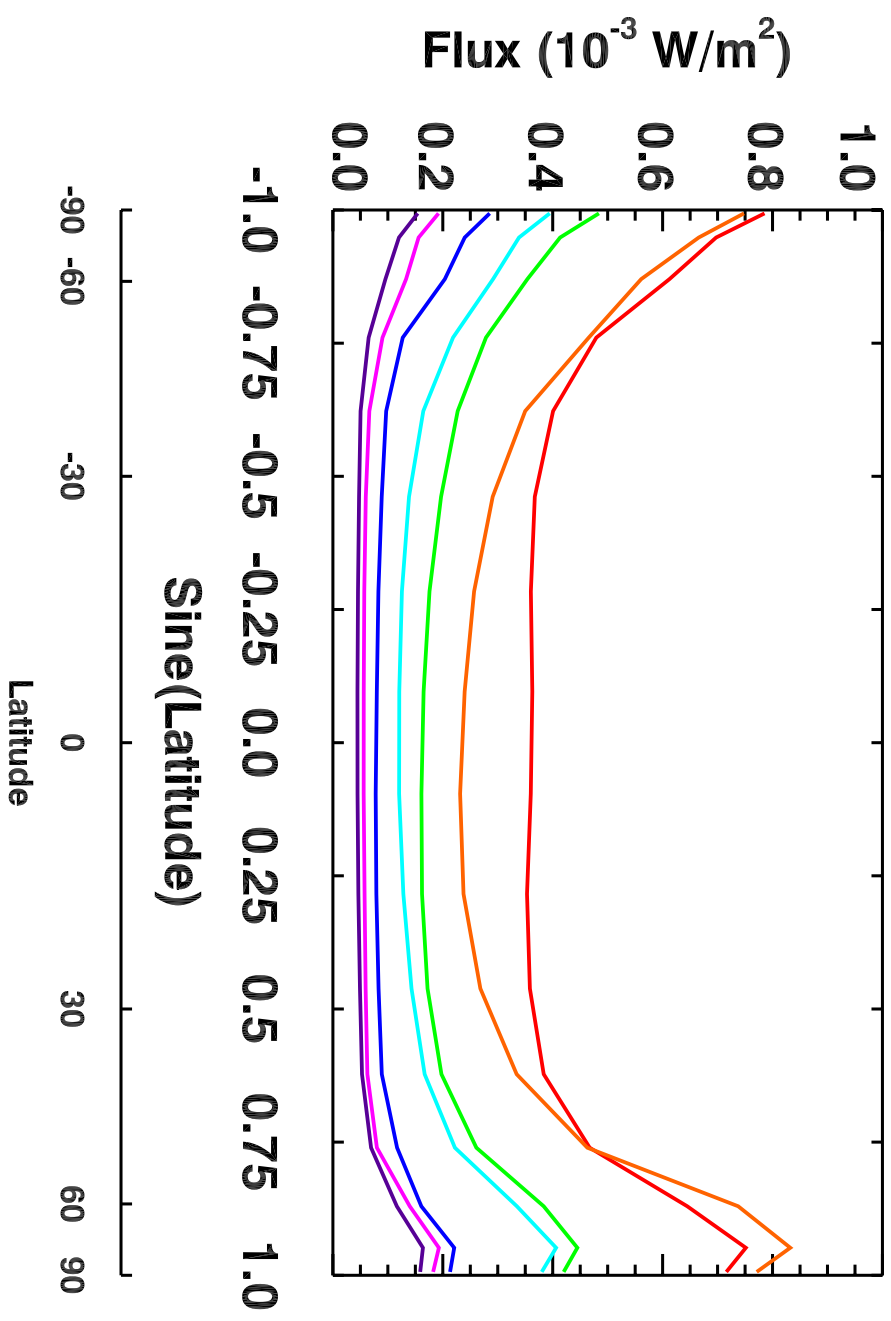
**ANNUAL AVERAGE CO2 INFRARED FLUX
Southern Hemisphere**

Milliwatts/m²



0.8 1.0 1.1 1.2 1.3 1.4 1.5 1.6 1.7 1.8 1.9 2.0 2.4

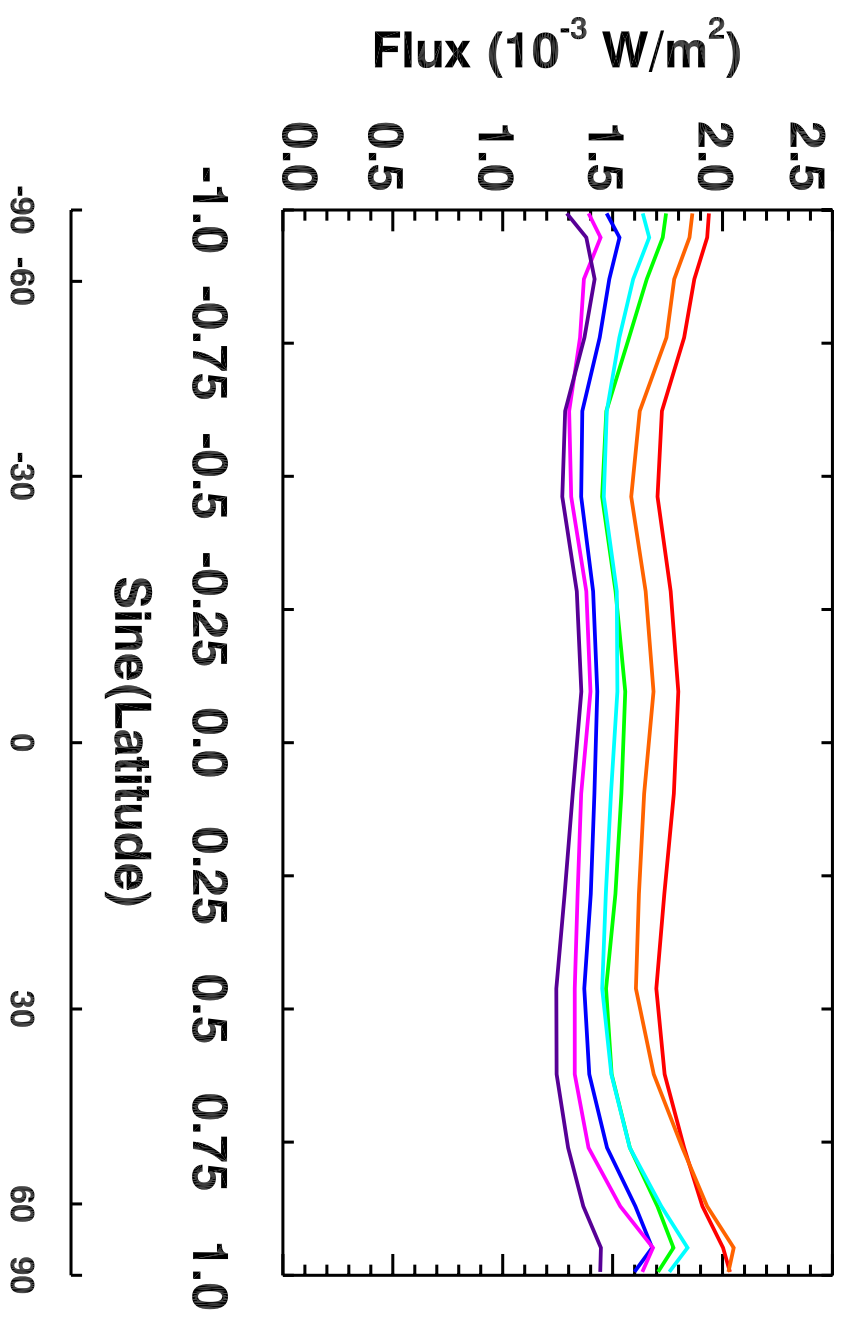
SABER NO Zonal Average Flux by Year



YEAR: 2002 2003 2004 2005 2006 2007 2008

Latitude

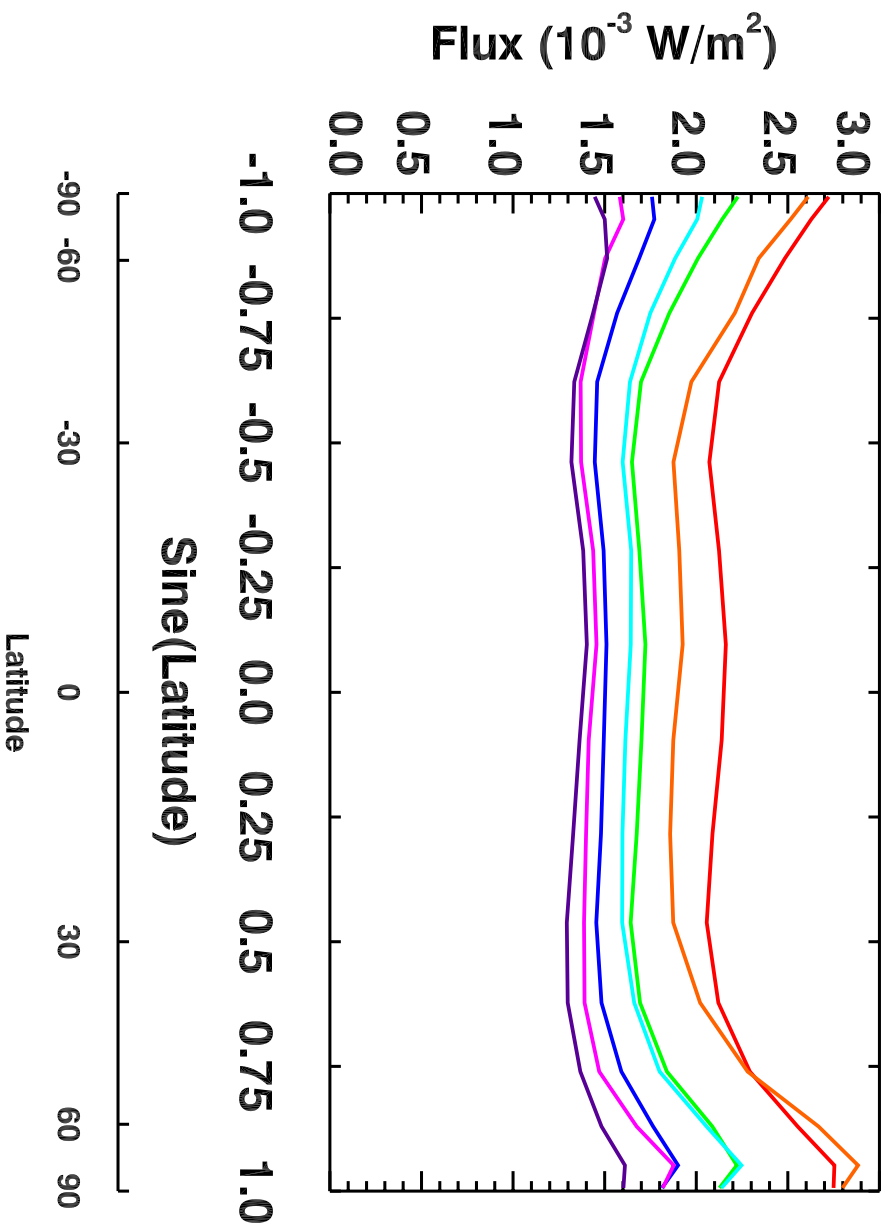
SABER CO2 Zonal Average Flux by Year



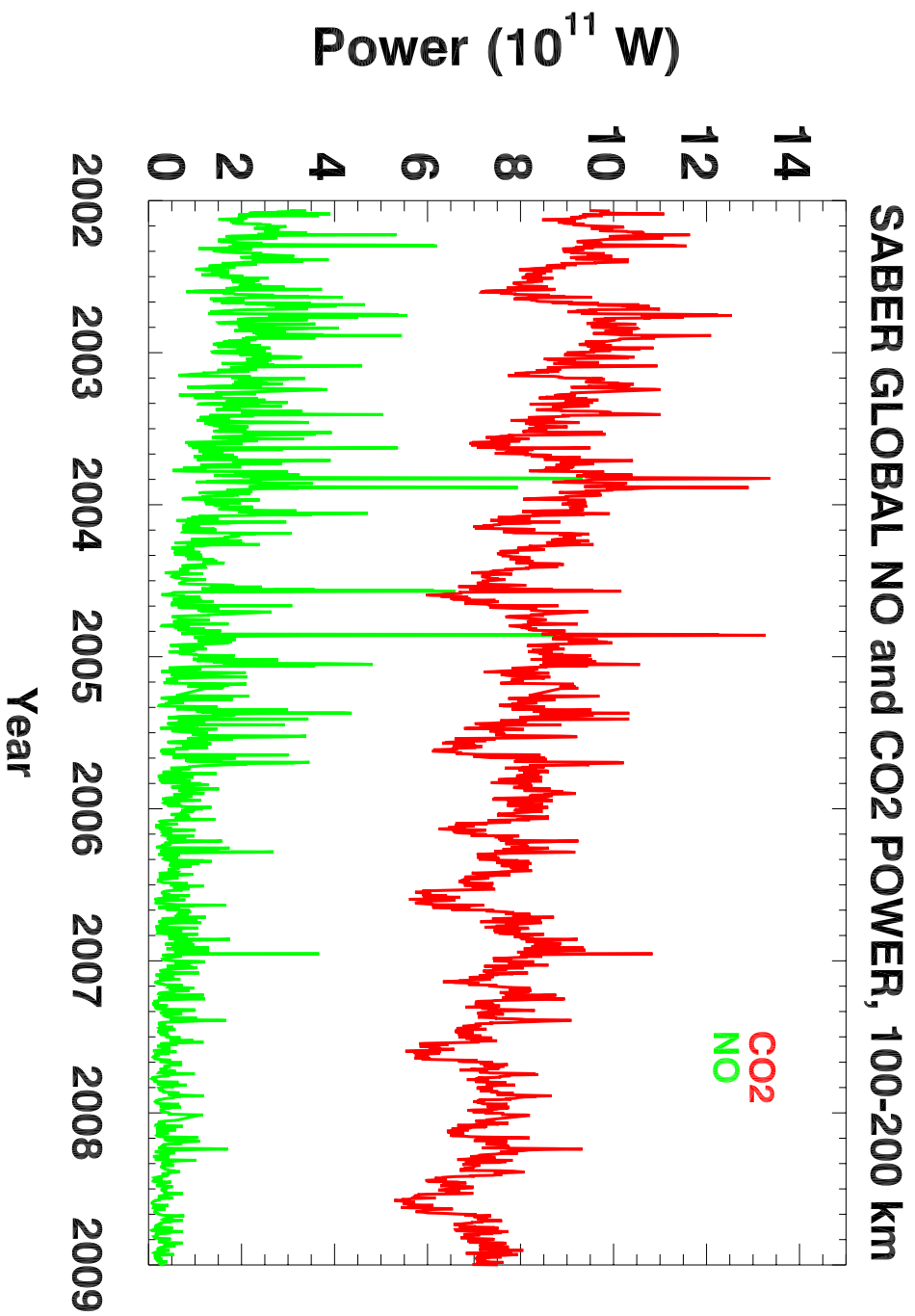
YEAR: 2002 2003 2004 2005 2006 2007 2008

Latitude

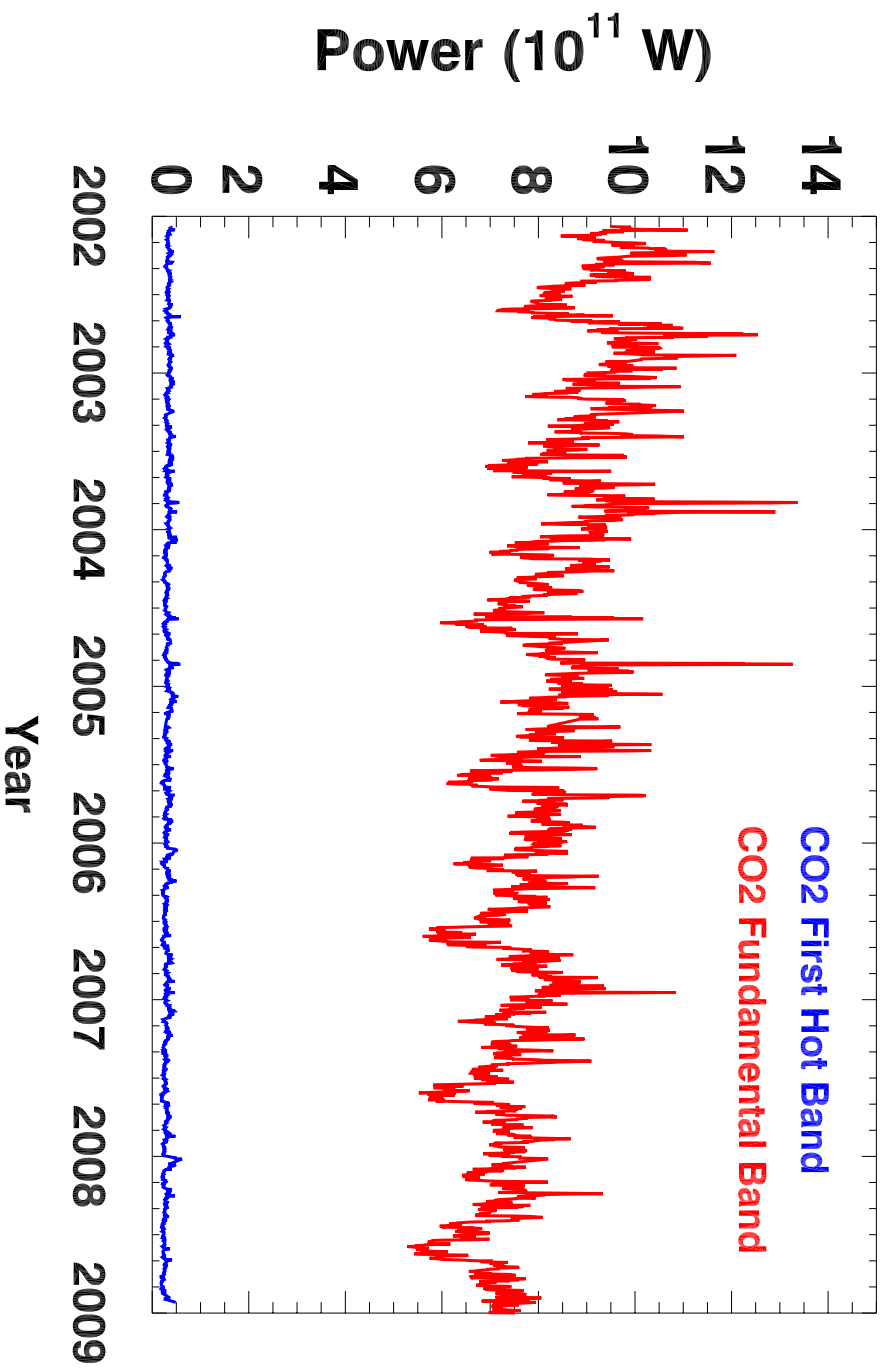
SABER Total Zonal Average Flux by Year



YEAR: 2002 2003 2004 2005 2006 2007 2008



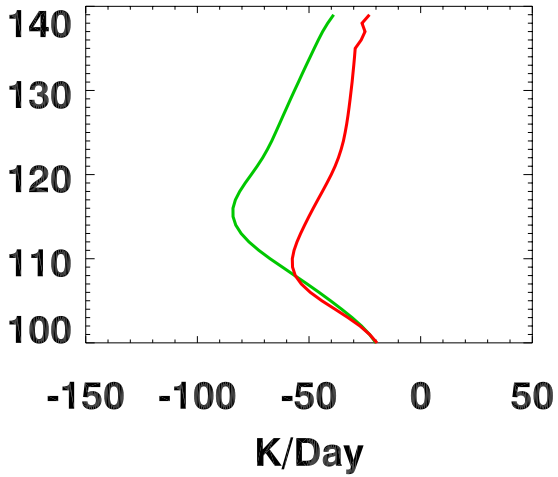
SABER GLOBAL CO2 POWER, 100-139 km



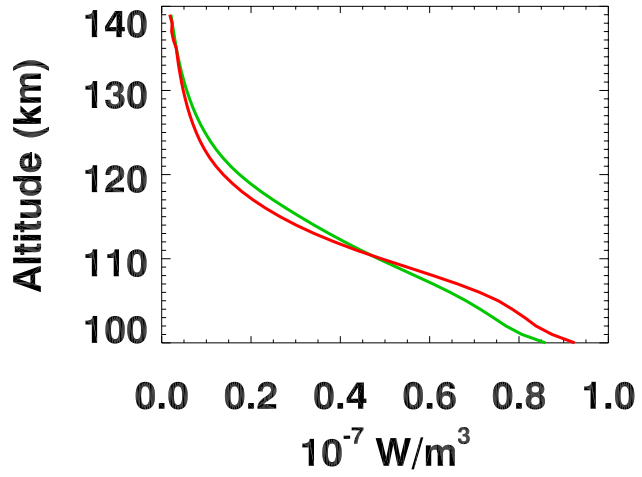
Nominal vs Sensitivity Test Results

Zonal Average for Latitudes 33N to 44N, 2008 Day 198

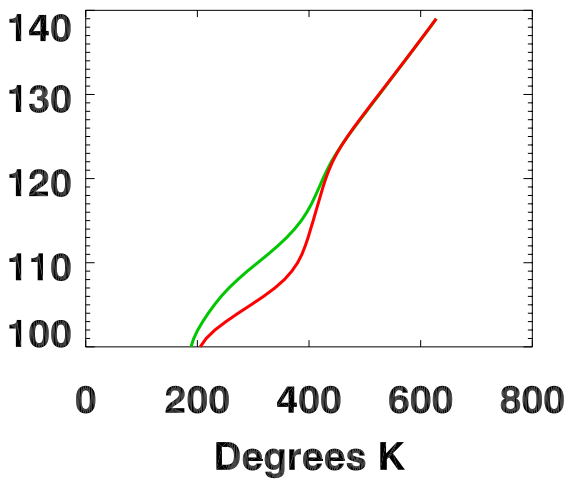
Cooling Rate



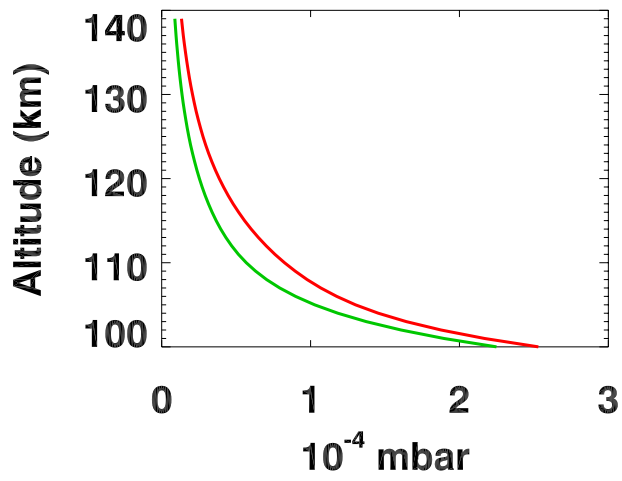
Cooling Rate (W/m^3)



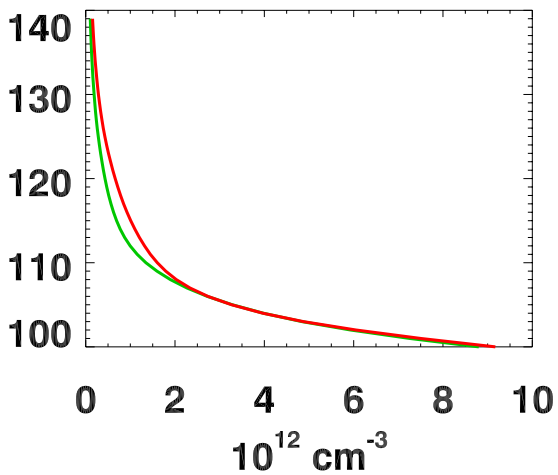
Temperature



Pressure



Density



NOMINAL

SENSITIVITY TEST